Large Gap Topological Insulator Bi_2Te_3 with a Single Dirac Cone on the Surface

Y. L. Chen,[1, 2, 3] J. G. Analytis,[1, 2] J. H. Chu,[1, 2] Z. K. Liu,[1, 2] S. K. Mo,[2, 3] X. L. Qi,[1, 2] H. J. Zhang,[4]
D. H. Lu,[1] X. Dai,[4] Z. Fang,[4] S. C. Zhang,[1, 2] I. R. Fisher,[1, 2] Z. Hussain,[3] and Z. X. Shen[1, 2]

[1]*Stanford Institute for Materials and Energy Sciences,*
SLAC National Accelerator Laboratory, 2575 Sand Hill Road, Menlo Park, California 94025
[2]*Geballe Laboratory for Advanced Materials, Departments of Physics*
and Applied Physics, Stanford University, Stanford, California 94305
[3]*Advanced Light Source, Lawrence Berkeley National Laboratory Berkeley California, 94720, USA*
[4]*Beijing National Laboratory for Condensed Matter Physics,*
and Institute of Physics, Chinese Academy of Sciences, Beijing 100190, China
(Dated: November 9, 2021)

We investigate the surface state of Bi_2Te_3 using angle resolved photoemission spectroscopy (ARPES) and transport measurements. By scanning over the entire Brillouin zone (BZ), we demonstrate that the surface state consists of a single non-degenerate Dirac cone centered at the Γ point. Furthermore, with appropriate hole (Sn) doping to counteract intrinsic n-type doping from vacancy and anti-site defects, the Fermi level can be tuned to intersect only the surface states, indicating a full energy gap for the bulk states, consistent with a carrier sign change near this doping in transport properties. Our experimental results establish for the first time that Bi_2Te_3 is a three dimensional topological insulator with a single Dirac cone on the surface, as predicted by a recent theory.

Soon after the theoretical prediction[1], a new state of quantum matter - the two-dimensional (2D) topological insulator displaying the quantum spin Hall(QSH) effect - was experimentally observed in the HgTe quantum wells[2]. The QSH state[3, 4] has an insulating gap in the bulk and gapless states at the edge where opposite spin states counter-propagate. The two opposite spin states form a single massless Dirac fermion at the edge, and the crossing of their dispersion branches at a time reversal invariant point is protected by the Kramers theorem. This robust protection is a consequence of the $Z2$ topological quantum number of the bulk quantum states[5]. The dissipationless edge state transport of the QSH state may enable low power spintronics devices.

A few years ago, 2D massless Dirac fermions were experimentally discovered in graphene with two inequivalent massless Dirac points for each spin orientation, giving rise to four copies of massless Dirac fermions in total. This is consistent with the experimentally observed quantized Hall conductance in units of $2e^2/h$[6], as each Dirac fermion leads to a quantized Hall conductance in units of $e^2/(2h)$ in an external magnetic field. It is no accident that graphene has an even number of massless Dirac fermions, since no time-reversal invariant purely 2D fermion system can have a single, or an odd number of massless Dirac fermions. Therefore, one can only observe a single Dirac fermion in a 2D system if it is the boundary of a three-dimensional (3D) system, called a 3D topological insulator[7, 8, 9, 10]. A 3D topological insulator has a bulk insulating gap with gapless surface states inside the bulk gap. In the simplest case, the surface state consists of a single Dirac cone, with one quarter the degrees of freedom of graphene. In this case, the electrodynamics of the topological insulator is described by an additional topological term in the Maxwell's equation[10], leading to striking quantum phenomena such as an image magnetic monopole induced by an electric charge[11].

The 3D material HgTe under strain is predicted to have a single Dirac cone on the surface[12]. However, experiments are difficult to perform under the strain condition. The $Bi_{1-\delta}Sb_\delta$ alloy is also predicted to be a 3D topological insulator in the narrow alloying content regime of $\delta = 0.07 \sim 0.22$[13, 14], and a recent ARPES study reveals the novel nature of the surface state despite its complexity, with as many as five branches crossing the Fermi level (E_F)[15]. However, the small bulk gap ($\sim 10meV$[16] or $\sim 50meV$[15]) makes it vulnerable to intrinsic random substitutional disorder, possibly leading to bulk impurity bands which can overlap with the surface states or smearing out of the bulk gap. Considering the lack of systematic doping dependent measurements, it is unclear whether the material is indeed insulating in the bulk. Furthermore, the small gap system is not well suited for realistic high(room) temperature applications.

Recently, a new class of stoichiometric materials, Bi_2Te_3, Bi_2Se_3 and Sb_2Te_3 has been theoretically predicted to be 3D topological insulators whose surface states consist of a single Dirac cone at the Γ point[17]. In a recent ARPES experiment[18] on Be_2Se_3, a single surface electron pocket with a Dirac point below the Fermi level at the Γ point was reported. However, a deep bulk electron pocket coexisting with the topologically non-trivial surface states was also observed in the same experiment. Therefore, the topological insulating behavior in this class of materials is yet to be established experimentally.

In this letter, we use ARPES and transport experiments to investigate both the bulk and surface state

electronic properties of $(Bi_{1-\delta}Sn_\delta)_2Te_3$ crystals (where δ represents nominal Sn concentration, incorporated to compensate n-type doping from vacancy and anti-site defects. By scanning over the entire Brillouin zone, we confirm that the surface states consist of a single, non-degenerate Dirac cone at the Γ point. At appropriate doping ($\delta = 0.67\%$), we found that the bulk states disappear completely at the Fermi level, thus realizing for the first time the topological insulating behavior in this class of materials. With a much larger bulk band gap ($165meV$) compared to the energy scale of room temperature($24meV$), the topological protection of the surface states in this material could lead to promising applications in low power spintronics devices at room temperature.

Fig. 1 summarizes the bulk and surface electronic structures and Fermi-surfaces (FSs) topology of undoped Bi_2Te_3. The crystal structure of Bi_2Te_3 (Fig. 1a) is of the tetradymite type, formed by stacking quintuple layer groups sandwiched by three sheets of Te and two sheets of Bi within each group[19]. *Ab initio* calculations predict that the undoped Bi_2Te_3 is a semiconductor (Fig. 1b), and that the Fermi-surface(Fig. 1c) from bulk conduction band(BCB) projected onto the surface Brillouin zone(BZ) exhibits triangular or hexagonal snowflake-like electron pocket centered at the Γ point (Fig. 1c) depending on its k_z position in reciprocal space.

Actual band dispersions measured by the ARPES experiment along two high symmetry directions are shown in Fig 1d. In addition to the broad spectra of the bulk electron pocket on top and the "M" shape valance band at bottom as predicted in the *ab initio* calculation, there is an extra sharp "V" shape dispersion resulted from the surface state. The linear dispersion in both plots clearly indicates a massless Dirac Fermion with a velocity of $4.05 \times 10^5 m/s(2.67eV \cdot \mathring{A})$ and $3.87 \times 10^5 m/s(2.55eV \cdot \mathring{A})$ along the $\Gamma - K$ and $\Gamma - M$ directions respectively, which are about 40% of the value in graphene[6] and agree well with our first principle calculation (by the method described in[17]) which yields 2.13 and 2.02 $eV \cdot \mathring{A}$ along the $\Gamma - K$ and $\Gamma - M$ directions, respectively.

This sharp surface state also forms a FS pocket in addition to the calculated FS from bulk bands. As shown in Fig. 1e, 1f(ii), in each BZ there is a hexagram FS enclosing the snowflake like bulk FS. A broad FS map covering three adjacent BZs (Fig. 1e) confirms that there is only one such hexagram FS resulting from the "V" shape Dirac-type surface state in each BZ. It should be noted that the spin-orbit coupling (SOC) in this material is rather strong and the atomic SOC of Bi-6p orbital is $\lambda = 1.25eV$[17], about twice of that in Au ($\lambda = 0.68eV$)[20]. Given that our energy and momentum resolution ($\delta E < 0.016eV$ and $\delta k < 0.012(1/\mathring{A})$) is better than needed to resolve even the much smaller Au surface state splitting ($\Delta E = 0.11eV, \Delta k = 0.023(1/\mathring{A})$)[21], The fact that we never observe more than one set of surface
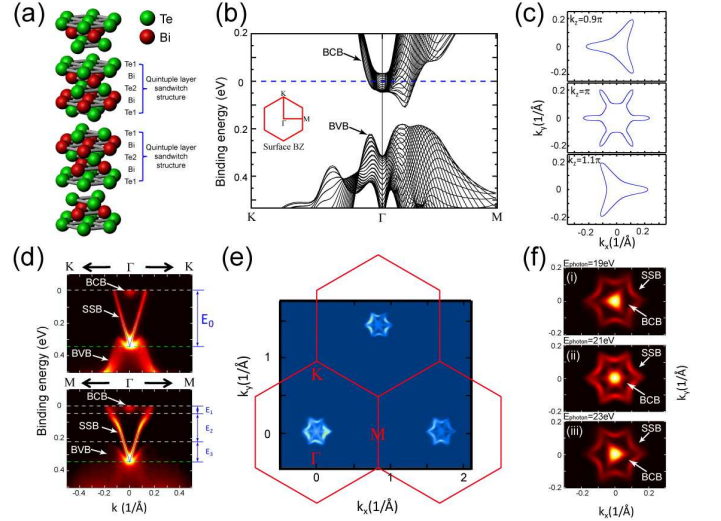

FIG. 1: (Color) Crystal and electronic structures of Bi_2Te_3 (a) Tetradymite-type crystal structure of Bi_2Te_3, formed by stacking quintuple-layer groups sandwiched by three sheets of Te and two sheets of Bi. (b) Calculated bulk conduction band(BCB) and bulk valance band(BVB) dispersions along high symmetry directions of the surface BZ (see inset), with the chemical potential rigidly shifted to 45meV above the BCB bottom at to match the experimental result. (c) The k_z dependence of the calculated bulk FS projection on the surface BZ. (d) ARPES measurements of band dispersions along $K-\Gamma-K$(top) and $M-\Gamma-M$ (bottom) directions. The broad bulk band (BCB and BVB) dispersions are similar to those in panel (b), while the sharp V-shape dispersion is from the surface state band (SSB). Energy scales of the band structure are labeled as: E_0: Binding energy of Dirac point (0.34eV), E_1: BCB bottom binding energy(0.045eV), E_2:bulk energy gap(0.165eV) and E_3: energy separation between BVB top and Dirac point (0.13eV). (e) Measured wide range FS map covering three BZs shows that the FSs only exist around Γ point, where the red hexagons represent the surface BZ. The uneven intensity of the FSs at different BZs results from the matrix element effect. (f) Photon energy dependent FS maps. The shape of the inner FS changes dramatically with photon energies, indicating a strong k_z dependence due to its bulk nature as predicted in panel (c), while the non-varying shape of the outer hexagram FS confirms its surface state origin.

state in all dopings and under all experimental conditions - including different photon energies, polarizations and two experimental setups in different synchrotrons – rules out the possibility that the Dirac cone is spin degenerated. This crucial observation clearly demonstrates that Bi_2Te_3 is the ideal candidate as the parent compound for the simplest kind of 3D topological insulator[17] - a simplicity resembling that of the hydrogen atom in atomic physics. In contrast, graphene has two valleys with spin degeneracy, totaling four Dirac cones in each BZ, leading to a topological trivial state. Furthermore, since there is only one surface Fermi pocket in each surface BZ, surface state will only cross the Fermi level *once* between and M, rather than the complex crossing of *five* times

as observed in $Bi_{0.9}Sb_{0.1}$[3, 15].

The surface nature of the hexagram FS resulting from the sharp "V" shape dispersion is further established by a photon energy dependence study (Fig. 1f). By varying the excitation photon energy, the shape of the snowflake-like bulk FS changes from a left pointing triangle(Fig. 1f(i)) to a right pointing triangle(Fig. 1f(iii)) as a result of the k_z dispersion of the 3D bulk electronic structure as illustrated in Fig. 1c. In contrast, the shape of the hexagram-like FS does not change with the incident photon energy, confirming its two dimensional nature (i.e. no k_z dispersion). We note that the perfect Bi_2Te_3 single crystal is predicted to be a bulk insulator. The electron carriers observed in our experiment arise from crystal imperfections, specifically vacancies and anti-site defects [22]. Given the substantial bulk gap (Fig. 1d), one can tune the E_F into the gap by doping holes to compensate the electron carriers, thus realizing the topological insulator phase in this material. In order to lower the Fermi level into the bulk gap, we introduce controlled Sn doping into Bi_2Te_3. As a Sn atom has one less valence electron than a Bi atom, substituting Bi by Sn effectively dopes holes into the compound, which decreases the bulk electron density and results in a downshift of E_F[23]. The effect of Sn doping is clearly demonstrated in Fig. 2, where the FSs and band dispersions of samples of four different nominal dopings ($0\%, 0.27\%, 0.67\%$, and 0.9%) are shown from panel (a) to (d), respectively. The top row shows the evolution of the FSs. The surface state FS pocket is observed in all four compounds, whose volume shrinks with increasing doping, with its shape varying from a hexagram ($0\%, 0.27\%$ and 0.67% dopings) to an hexagon (0.9% doping). The evolution of the bulk FS is more complicated. For the 0% and 0.27% doped samples, there is a bulk electron pocket inside the hexagram surface state FS, with its size smaller for the 0.27% doped sample. For 0.67% doped sample, the bulk electron pocket FS completely vanishes, leaving no other FSs besides the surface state FS. For the 0.9% doped sample, on the contrary to 0% and 0.27% doped samples, there are six leaves-like hole pockets outside the hexagon surface stat FS, rising from the top of the bulk valence band(BVB).

The evolution of the band dispersion with doping is further illustrated in the middle row of Fig. 2, where the Dirac points (determined by the crossing point of the fit linear dispersions of the "V" shape surface states (SS)) from all four doping samples are aligned to highlight the down-shift of E_F due to the hole (Sn) doping. In undoped Bi_2Te_3 (Fig. 2a(i), since E_F lies at 0.34eV above the Dirac point and the BCB bottom is only 0.295eV above it, E_F intersects both the SS and BCB bands, resulting in a hexagram and a snowflake FS pocket, respectively. In 0.27% doped sample (Fig. 2b(ii)), while E_F is lowered by 20meV due to Sn doping, it still lies above the BCB minimum, thus both FS pockets from SS
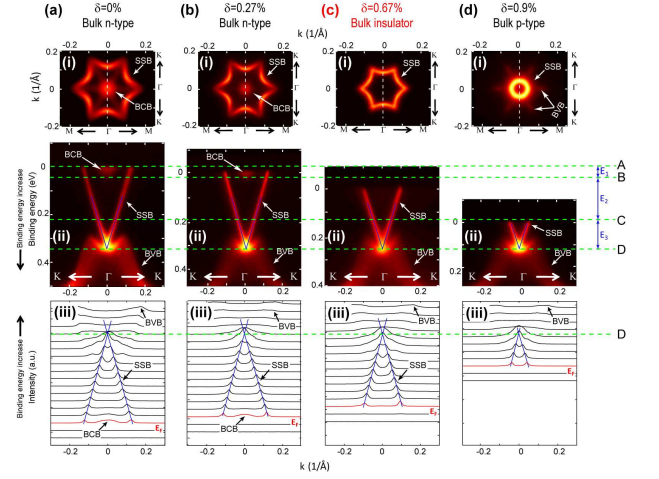

FIG. 2: (Color) Doping dependence of FSs and E_F positions. (a)-(d): Measured FSs and band dispersions for $0\%, 0.27\%, 0.67\%$ and 0.9% nominally doped samples. Top row: FS topology (symmetrized according to the crystal symmetry); Middle row: Image plots of band dispersions along $K-\Gamma-K$ direction as indicated by white dashed lines superimposed on the FSs in the top row. Bottom row: Momentum distribution curve (MDC) plots of the raw data. Definition of energy positions: A: E_F position of undoped Bi_2Te_3, B: BCB bottom, C: BVB top and D: Dirac point position, determined by the intersection of the fitted linear dispersions. Energy scale $E_1 \sim E_3$ are defined in Fig. 1d.

and BCB still exist, although with smaller volumes as a result of the lowered E_F. For the 0.67% doped sample (Fig. 2c(ii)), significantly, E_F is now further downshifted and resides between the BCB bottom and the BVB top, therefore the FS pockets associated with the bulk states completely vanish and the only FS pocket left is the one originated from the SS(Fig. 2c(i)). This is exactly what one should expect for a topological insulator. With further hole doing (0.9%, Fig. 2d(ii)), E_F is further shifted downward and resides at 0.12eV above the Dirac point, slightly below the BVB top which is 0.13eV above the Dirac point (E_3 in Fig. 1d(ii)). As a consequence, the bulk hole pockets emerge in the FS map in Fig. 2d(i) as the six "leaves" outside the SS FS. For all doping levels, we have confirmed from photon energy dependence ARPES that only the V-shape dispersion comes from the surface state while other features are resulted from bulk states.

The third row of Fig. 2 shows the stack plots of raw momentum distribution curves (MDCs) for the band dispersions shown in the middle row, which fully support the observations and conclusions above. The lineshape of the bulk states does not possess a sharp peak because of the final state effect arisen from the kz dispersion[24]; on the contrary, the surface state band(SSB) always exhibits sharp peak in the spectrum, again confirming its 2-D character.
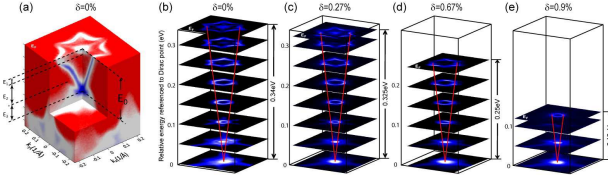
Unlike a simple circular Dirac cone, the observed sur-

FIG. 3: (Color) (a) 3D illustration of the band structures of undoped Bi_2Te_3, with the characteristic energy scales $E_0 \sim E_3$ defined in Fig. 1d. (b)$\sim$(d): Constant energy contours of the band structure and the evolution of the height of E_F referenced to the Dirac point for the four dopings. Red lines are guides to the eye that indicate the shape of the constant energy band contours, and intersect at the Dirac point.
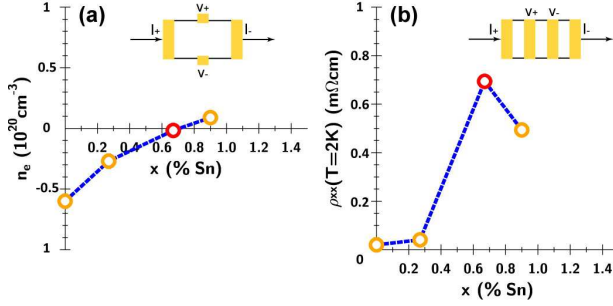

FIG. 4: (Color) Electric transport measurements on samples of four different dopings. (a) Carrier density determined by Hall coefficient measurement. Red symbol indicates the value for 0.67% doped sample, for which ARPES measurements show no bulk FS pocket (see text). (b) Resistivity measured by four-probe methods. Insets in (a), (b) show the measurement schematics.

face state in doped Bi_2Te_3 exhibits richer structure. As shown in Fig. 3, the 3D band structure (Fig. 3a) and the cross sections of the Dirac-like dispersion at various binding energies are demonstrated (Fig. 3(b-e)). When approaching the Dirac point from E_F, the shape of the SSB evolves gradually from a hexagram to a hexagon, then to a circle of shrinking volume, and finally converges into a point, the Dirac point, which is protected by the Kramers theorem. From the doping evolution of the Fermi surface topology, band dispersion, and the spectra lineshape shown above, we have found convincing evidence that the 0.67% Sn-doped Bi_2Te_3 is the long sought three dimensional strong topological insulator with a single Dirac cone and a large bulk band gap.

The observations of ARPES are also supported by electric transport measurements. From the Hall measurement (Fig.4a), an effective three-dimensional carrier density (ne) is extracted as a function of the Sn doping (Figure 4a). Evidently, at $\delta = 0.67\%$ there is a dramatic reduction in ne as the carrier type is inverted from n-type to p-type. Similarly the in-plane resistivity(Fig. 4b) exhibits an clear enhancement at $\delta = 0.67\%$. The peak at this intermediate doping indicates that the conductivity reduction is primarily due to a dramatic decrease in the

carrier density. The agreement between the ARPES and transport measurements confirms that Sn doping drives n-type Bi_2Te_3 into p-type, making Bi_2Te_3 an ideal parent for the 3D topological insulator.

Our results on Bi_2Te_3 clearly show its distinction and advantages over the previously studied material $Bi_{0.9}Sb_{0.1}$ and graphene: The single Dirac cone makes it the simplest model system for studying the physics of topological insulators. In particular, in order to observe the topological magneto-electric effect, a thin magnetic layer needs to be coated on the surface to break the time-reversal symmetry and create a full insulating gap at the Dirac point. Such effect is most likely to occur in a system with a single Dirac cone on the surface[25]. Furthermore, the large bulk gap points to great potential for possible high temperature spintronics applications on a 3D condensed matter system which is easy to be realized with current standard semiconductor technology.

[1] B. A. Bernevig, T. L. Hughes, S.-C. Zhang, Science 314, 1757 (2006)
[2] M. Konig et al., Science 318, 766 (2007)
[3] C. L. Kane, E. J. Mele, Phys. Rev. Lett. 95, 226801 (2005)
[4] B.A. Bernevig, S.-C. Zhang, Phys. Rev. Lett. 96, 106802 (2006)
[5] C. L. Kane, E. J. Mele, Phys. Rev. Lett. 95, 146802 (2005)
[6] Y. Zhang, et al., Nature 438 201 (2005)
[7] L. Fu, C. L. Kane, and E. J. Mele Phys. Rev. Lett. 98, 106803 (2007)
[8] J. E. Moore, L. Balents, Phys. Rev. B 75, 121306 (2007)
[9] R. Roy, preprint available at http://arxiv.org/abs/cond-mat/0604211v2
[10] X.-L. Qi, T. L. Hughes, S.-C. Zhang, Phys. Rev. B 78, 195424 (2008)
[11] X.-L. Qi, et al., Science 323, 1184 (2009)
[12] X. Dai, et al., Phys. Rev. B 77 125319
[13] L. Fu and C. L. Kane, Phys. Rev. B 76, 045302 (2007)
[14] J. C. Y. Teo, L. Fu, and C. L. Kane Phys. Rev. B 78, 045426 (2008)
[15] D. Hsieh, et al., Nature 452, 970 (2008)
[16] B. Lenoir, et al., J. Phys. Chem. Solids 57, 89 (1996)
[17] H. J. Zhang et al., preprint available at http://arxiv.org/abs/0812.1622

[18] Y. Xia, *et al.*, Preprint available at http://arxiv.org/abs/0812.2078v1

[19] Wyckoff, R. W. G.: Crystal Structures 2, J. Wiley and Sons, New York, 1964

[20] M. Vijayakumar and M. S. Gopinathan, J. Mol. Struct, 361, 15(1996)

[21] S. LaShell, B.A. McDougall, and E. Jensen, Phys. Rev. Lett. 77, 3419 (1996)

[22] C. B. Saiterthwaite and R. W. Ure Jr., Phys. Rev., 108, 1164 (1957)

[23] V. A. Kulbachinskii *et al*. Phys. Rev. B, 59, (1994), 16921

[24] T. Miller and T.-C. Chiang, J. Phys.: Condens. Matter 13 (2001) 11115

[25] Qin Liu, *et al*, preprint available at http://arxiv.org/abs/0808.2224